

## Article

# Experimental Investigation of the Frequency Response of an LC-Filter and Power Transformer for Grid Connection

Christoffer Fjellstedt , Johan Forslund  and Karin Thomas

Division of Electricity, Department of Electrical Engineering, Uppsala University, 752 37 Uppsala, Sweden  
\* Correspondence: christoffer.fjellstedt@angstrom.uu.se

**Abstract:** The power delivered by a voltage source inverter needs to be filtered to fulfill grid code requirements. A commonly used filter technology is the LCL-filter. An issue with the LCL-filter is the occurrence of a resonance peak, which can be mitigated with active or passive damping methods. The transfer function of the filter is often used to investigate the frequency response of the system and propose damping methods. The use of an LC-filter combined with a power transformer to form an LCL-filter has not been extensively investigated. Therefore, the study in this article introduces a model for an LC-filter and power transformer for the grid connection and a derived transfer function for the model. The transfer function for the system is validated with simulations and experimental investigations. The results from simulations and the results from a direct solution of the derived analytical function overlap almost perfectly. The magnitudes of the experimental results are approximately 1 dB lower than the simulation and analytical results before the resonance frequency. At the resonance frequency, the experimental results are approximately 13.4 dB lower. The resonance frequency, however, occurs at approximately the same frequency. It is also concluded that the system is significantly damped.

**Keywords:** LC-filter; LCL-filter; power transformer; grid connection; renewable energy



**Citation:** Fjellstedt, C.; Forslund, J.; Thomas, K. Experimental Investigation of the Frequency Response of an LC-Filter and Power Transformer for Grid Connection. *Energies* **2023**, *16*, 5784. <https://doi.org/10.3390/en16155784>

Academic Editor: Javier Contreras

Received: 30 June 2023

Revised: 24 July 2023

Accepted: 25 July 2023

Published: 3 August 2023



**Copyright:** © 2023 by the authors. Licensee MDPI, Basel, Switzerland. This article is an open access article distributed under the terms and conditions of the Creative Commons Attribution (CC BY) license (<https://creativecommons.org/licenses/by/4.0/>).

## 1. Introduction

As the demand for renewable energy increases, the level of renewable energy sources connected to the electrical grid is expected to increase dramatically [1]. A common characteristic of renewable energy sources is that the interface with the electric grid needs to be achieved with power electronic converters. This is often the case for wind power and is always necessary for photovoltaic power sources [2,3]. Ocean renewable energy sources such as marine current power and wave power will also require a power electronic stage before the grid connection. The grid interface is often achieved with a power inverter, where the inverter voltages need to be filtered to fulfill grid code requirements and reduce stress on the components of the grid connection. A typical grid connection for renewable energy consists of a rectifying stage and an inverter stage. Figure 1 shows the electrical system used in the experimental small-scale marine current power station in Söderfors, Sweden, operated by Uppsala University [4]. This setup is used as a reference for the work regarding components of the grid connection in this paper. The electrical system at the test site consists of a back-to-back converter with a two-level voltage source converter on the generator side and a three-level voltage source converter on the grid side [5,6]. The grid-side converter is connected to the grid through an LCL-filter constructed by an LC-filter and the inductance of a power transformer. The purpose of the filter is to improve the quality of the power injected into the grid, and the purpose of the transformer is to increase the voltage from the inverter and to electrically isolate the inverter from the grid.

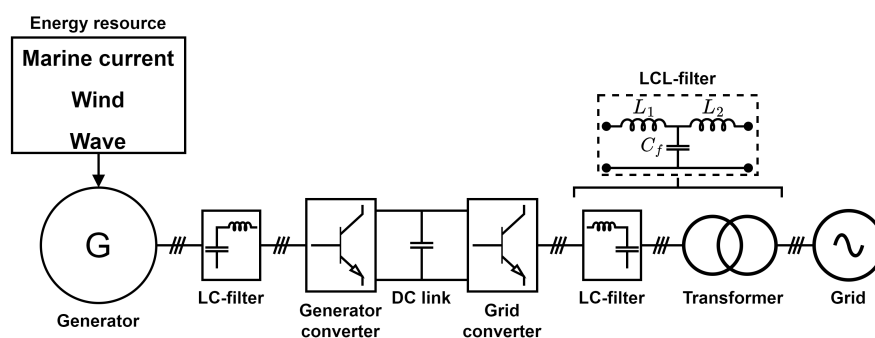


**Figure 1.** A back-to-back power converter.

A large variety of active and passive filter technologies can be found in the literature [7–9]. A single inductor, a so-called L-filter, is a first-order filter and, with regards to the number of components and the complexity, one of the simplest filter technologies. However, the L-filter has a lower high-frequency harmonics-attenuation rate compared to other filter technologies, and a large inductor is usually required, which makes the construction bulky [8]. An extension is to include a capacitor and thus make an LC-filter, which is a second-order filter. The LC-filter has a higher high-frequency attenuation rate than the L-filter [8]. If another inductor is used, the filter becomes a third-order filter, named an LCL-filter, which has a substantially higher high-frequency attenuation rate compared to the L- and LC-filters. An advantage with LCL-filters is also that the components can be made smaller while the filter still has a superior attenuation rate compared to the L- and LC-filter [8].

The use of LCL-filters in the context of voltage source converters has been extensively investigated in the literature. In [10], for example, a step-by-step guide on how to design a voltage source converter with an LCL-filter is proposed. Essentially the same group of authors proposed, in another frequently cited paper, a method for designing the LCL-filter of a three-phase active rectifier [11]. The main goal of the method is to reduce the switching frequency ripple while keeping the costs at a reasonable level and achieving a high-performing rectifier. Other approaches to the design of voltage source converters with LCL-filters can be found in the literature. In [12], for example, an iterative design method for an L- and LCL-filter is proposed. In this method, the analytical expressions of the harmonic voltages of the converter based on Bessel functions are used to determine filter parameters that result in sufficient damping of the grid current harmonics. The proposed design method can also be based on a more specific energy source. To mention one example, the design procedure for LCL-filters for medium-voltage and megawatt voltage source converters with low switching frequency in wind turbines is discussed in [13]. In this study, a central aim of the design procedure is to minimize the physical size and weight of the components given a maximum limit of the switching frequency of the converter and specific limits on harmonics in the grid-side currents. In another energy source specific case, the design and control of an LCL-filter interfaced voltage source converter for a grid-connected photovoltaic source are discussed in [14]. More generalized studies can also be found in the literature. In [15], a design methodology for three-phase grid-connected voltage source converters for small- and medium-scale distributed energy sources is proposed. In this study, the effect of connecting the capacitors in a wye or delta configuration was also considered. In paper [16], a design method for an LCL-filter with optimum capacitance value based on reactive compensation is proposed. In [17], a design method in order to achieve an optimal LCL-filter design for two-level voltage source converters is presented.

A characteristic of the studies discussed above is that the occurrence of a resonance peak in the frequency response of the system due to the LCL-filter needs to be considered in the design. Damping strategies to attenuate the peak is an area that has been subject to much research [18]. One approach is passive damping, which is based on the inclusion of passive elements in the system, such as resistors [19,20]. Another approach is active

damping, where the control structure of the system is modified to achieve a damped system [19–21]. The active damping schemes can broadly be divided into strategies that do or do not require extra sensors [21]. A sensorless Kalman-filter-based active damping method is proposed in [22]. For the design of LCL-filters, magnetic integration has also been considered in the literature, where a filter and transformer are constructed on the same core [23–26]. Since the magnetic components are often large and heavy, integrating the filter and the transformer on the same core makes the system arguably less bulky and more energy-efficient [23]. As already mentioned, an aspect that is often considered for LCL-filter-based voltage source converters is the influence of the resonance peak on the control of the system. The study of this type of issue is often partially or entirely based on an analysis of the transfer function of the system, either with grid current feedback or inverter current feedback, where the transfer function is used for the development and understanding of damping and control strategies [9,19,20,27,28].

The use of an LC-filter combined with a power transformer to construct an LCL-filter, for example, the design at the Uppsala University test site in Söderfors, has, however, not been extensively investigated in the literature. The derivation and validation of system transfer functions have mostly been aimed at ideal lossless LCL-filters, filters with losses, and filters with various damping strategies [8,9,20]. A transfer function for the combination of an LC-filter and a power transformer that is not magnetically integrated has not been proposed and has not otherwise been extensively investigated. In order to design a suitable controller for a grid connection system, it is necessary to have an understanding of the frequency response of the considered system. A transfer function can contribute to giving this understanding and allowing the system designer to choose suitable control methods and, if necessary, damping methods. The purpose of the study presented in this article is therefore to give a comprehensive analysis of the concept of using an LC-filter and a power transformer as separate components to construct an LCL-filter. More specifically, a transfer function for an LC-filter and a power transformer using the inverter output voltage and the grid current is presented. The transfer function is validated by comparing the frequency response of the analytical solution with simulations and experimental measurements.

The paper is organized as follows: In Section 2, the three basic filter technologies, L-, LC-, and LCL-filters, are discussed. In Section 3, a common model of a non-ideal power transformer is presented, and in Section 4 the proposed model for the combination of an LC-filter and a power transformer is introduced, and the derivation of the transfer function for this system is presented. The method for validating the proposed model through simulations and experiments is presented in Section 5, and the results of the study are given in Section 6. Finally, the most important conclusions of the study are given in Section 7.

## 2. L-, LC-, and LCL-Filters

Single-phase equivalent circuits for the three common filter designs, L-, LC-, and LCL-filters, are shown in Figure 2. The main purpose of the filters in the context of grid-connected voltage source converters is to improve the quality of the power injected into the grid by attenuating high-frequency ripple, which usually arises from the PWM modulation of the voltage source converters [8,9]. The simplest design is the L-filter, since it only consists of one component, the inductor  $L$  with the impedance  $Z_L = sL$  in the Laplace domain [9]. In order to meet grid standards, a high inductance value is usually necessary, which makes the filter bulky and implies a large voltage drop and slow time response of the filter [9]. The L-filter is therefore not commonly considered as a feasible option for the grid connection of voltage source converters [9]. The frequency dynamic of the L-filter is usually analyzed with the transfer function derived from the input voltage,  $V_{in}$ , which corresponds to the output voltage from the inverter, to the current injected into the grid,  $I_{out}$ . If the grid voltage is assumed to be zero,  $V_{out} = 0$ , the Laplace transform of the transfer function is given by the following equation:

$$H_L = \frac{I_{out}}{V_{in}} = \frac{1}{sL_1}. \quad (1)$$

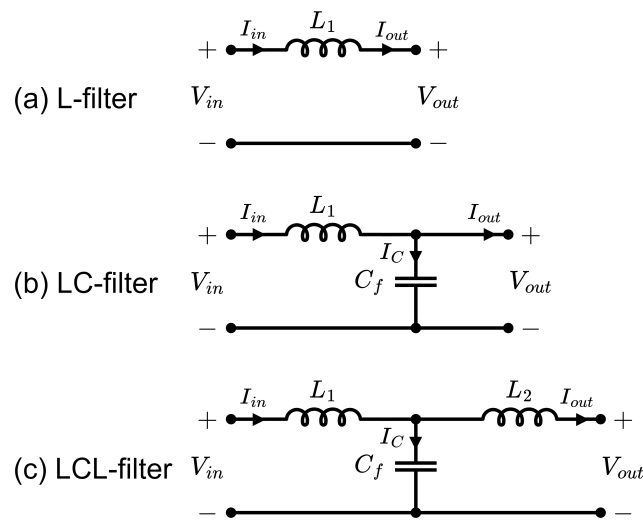


**Figure 2.** Single-phase equivalent circuits for the (a) L-filter, (b) LC-filter, and (c) LCL-filter.

The L-filter has an attenuation rate of  $-20$  dB/dec, as illustrated in Figure 3. An extension of the L-filter is to include a shunt-connected capacitor,  $C$ , in order to create a low-impedance route for high-frequency harmonics. The LC-filter is illustrated in Figure 2, and the frequency response of the filter is usually analyzed with the transfer function from the output voltage from the inverter,  $V_{in}$ , to the grid side voltage,  $V_{out}$ , while assuming the grid current to be zero,  $I_{out} = 0$ . This transfer function is given by the following equation:

$$H_{LC} = \frac{V_{out}}{V_{in}} = \frac{1}{L_1 C_f s^2 + 1}. \quad (2)$$

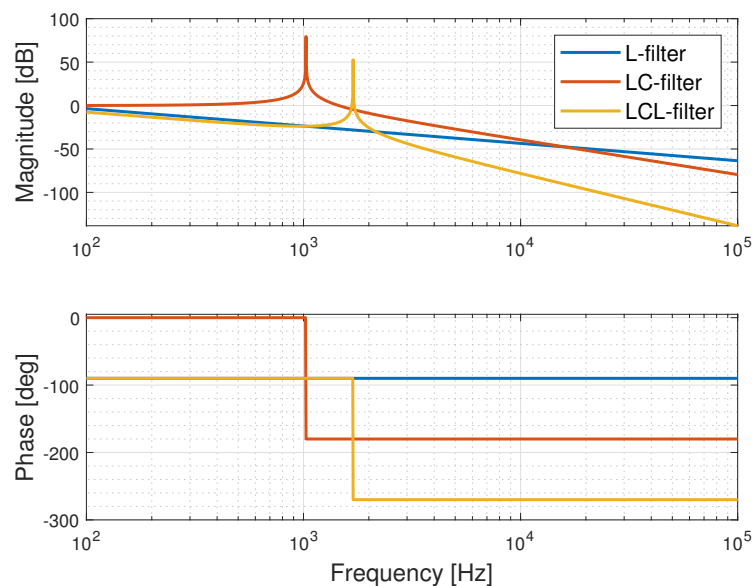


**Figure 3.** Bode plot for L-, LC-, and LCL-filters' transfer functions for a generic selection of filter parameters.

The LC-filter has a higher attenuation rate at high frequencies compared to the L-filter with  $-40$  dB/dec. From Figure 3, it can, however, be observed that the LC-filter has a resonance peak at a certain frequency. The resonance frequency is given by

$$\omega_{res,LC} = \frac{1}{\sqrt{L_1 C_f}}. \quad (3)$$

If another inductor is connected in series with an LC-filter, an LCL-filter is formed. The transfer function used for analyzing an LCL-filter is often from the output voltage from the inverter,  $V_{in}$ , to the current injected into the grid,  $I_{out}$ , while assuming the grid voltage to be zero,  $V_{out} = 0$ . The transfer function for the LCL-filter is given by the following equation:

$$H_{LCL} = \frac{I_{out}}{V_{in}} = \frac{1}{L_1 L_2 C_f s^3 + (L_1 + L_2) s}. \quad (4)$$

The attenuation rate of high-frequency harmonics is for the LCL-filter  $-60$  dB/dec, which is higher than both the L- and LC-filter. Similar to the LC-filter, the LCL-filter exhibits a resonance frequency at a certain frequency, which is given by

$$\omega_{res,LCL} = \sqrt{\frac{L_1 + L_2}{L_1 L_2 C_f}}. \quad (5)$$

### 3. Non-Ideal Power Transformer Model

The purpose of the transformer is to adapt the converter output voltage to the voltage level of the grid connection point and to galvanically isolate the converter from the grid. A common equivalent circuit representation of a non-ideal transformer is shown in Figure 4. The model consists of the following parts:

- An ideal transformer with a turns ratio  $n = N_1/N_2 = V_1/V_2$ .
- The primary- and secondary-side leakage inductance,  $L_p$  and  $L_s$ .
- The primary- and secondary-side copper resistance of the windings,  $R_p$  and  $R_s$ .
- The core losses,  $R_c$ , which incorporate the losses due to hysteresis and eddy currents in the core.
- The magnetizing inductance,  $L_m$ , which models the magnetization of the core material.

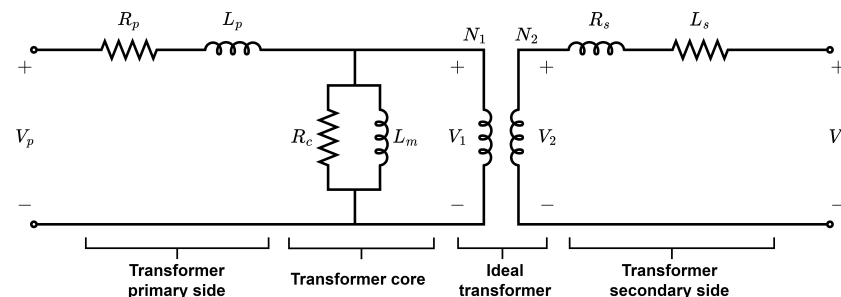


Figure 4. Single-phase transformer equivalent circuit model.

### 4. LC-Filter and Power Transformer Model

The focus of this article is to present a transfer function of an LC-filter and a power transformer that together form an LCL-filter. The derived transfer function will be validated by comparing the analytical frequency response with simulations and experimental results. The previously described LC-filter and transformer circuits are connected together, as shown in Figure 5. The output voltage from the inverter is represented by a voltage source  $V_{in}$ . The inductor in the LC-filter is represented by the inductance  $L_f$  and the resistance of the inductor  $R_f$ . The capacitive part of the filter is represented by  $C_f$ . The resistance of a capacitor is usually small and can therefore be disregarded for the analysis of the transfer function of the system [29]. The filter is connected to the secondary side of the transformer. For the purpose of modeling, all parts of the transformer are referred to the secondary side of the transformer. The primary side leakage inductance and series resistance, referred to the secondary side of the transformer, are represented by  $R'_p$  and  $L'_p$ , respectively. The core resistance and magnetization inductance, referred to the secondary side, are given by  $R'_c$  and  $L'_m$ , respectively. Finally, the circuit is connected to the grid on the primary side of the transformer, and the grid current is also referred to the secondary side of the transformer.

The impedance of the components, referred to the secondary side, is given by  $Z'_p = Z_p/n^2$ , where  $Z_p = R_p + sL_p$  and the current is calculated by  $I'_g = I_g \cdot n$ .

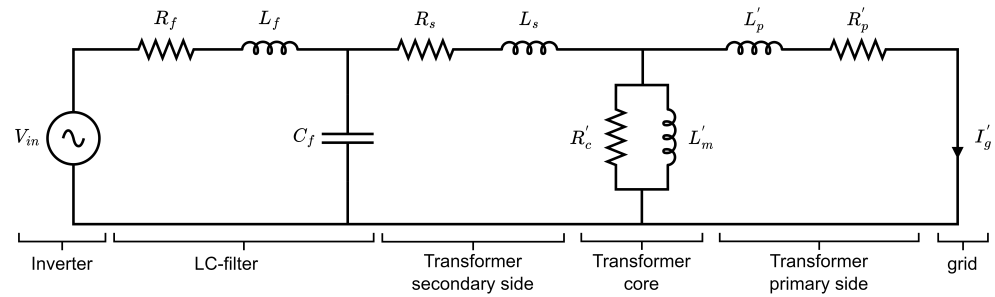


Figure 5. LC-filter and transformer model.

The frequency response of the system with grid current feedback is investigated. Therefore, a transfer function  $H_{LCT} = I_g/V_{in}$  is derived, where the grid current,  $I_g$ , is considered as the short-circuit current at the grid, and the inverter is represented by a sinusoidal voltage source,  $V_{in}$ . Expressing all parts of the circuit as impedances and using standard circuit theory, the transfer function can be shown to be expressed by the following equation:

$$H_{LCT} = \frac{I_g}{V_{in}} = \frac{1}{n} \cdot \frac{a_1 s^1}{b_5 s^5 + b_4 s^4 + b_3 s^3 + b_2 s^2 + b_1 s^1 + b_0 s^0}. \quad (6)$$

The coefficients in the numerator and the denominator are given by the following equations:

$$a_1 = R'_c L'_m, \quad (7)$$

$$b_0 = R'_c (R_f R'_p + R_s R'_p), \quad (8)$$

$$\begin{aligned} b_1 = & L'_m (R_f R'_p + R_s R'_p) \\ & + R'_c (R_f L'_p + L_f R'_p + C_f R_f R_s R'_p + R_s L'_p + L_s R'_p) \\ & + L'_m R'_c (R_f + R_s + R'_p), \end{aligned} \quad (9)$$

$$\begin{aligned} b_2 = & L'_m (R_f L'_p + L_f R'_p + C_f R_f R_s R'_p + R_s L'_p + L_s R'_p) \\ & + R'_c (L_f L'_p + C_f R_f L_s R'_p + C_f L_f R_s R'_p + C_f R_f R_s L'_p + L_s L'_p) \\ & + L'_m R'_c (L_f + R_f R_s C_f + C_f R_f R'_p + L_s + L'_p), \end{aligned} \quad (10)$$

$$\begin{aligned} b_3 = & L'_m (L_f L'_p + C_f R_f L_s R'_p + C_f L_f R_s R'_p + C_f R_f R_s L'_p + L_s L'_p) \\ & + R'_c (C_f L_f L_s R'_p + C_f R_f L_s L'_p + C_f L_f R_s L'_p) \\ & + L'_m R'_c (R_f L_s C_f + L_f R_s C_f + C_f R_f L'_p + C_f L_f R'_p), \end{aligned} \quad (11)$$

$$\begin{aligned} b_4 = & L'_m (C_f L_f L_s R'_p + C_f R_f L_s L'_p + C_f L_f R_s L'_p) \\ & + R'_c (C_f L_f L_s L'_p) \\ & + L'_m R'_c (L_f L_s C_f + C_f L_f L'_p), \end{aligned} \quad (12)$$

$$b_5 = C_f L_f L_s L'_p L'_m. \quad (13)$$

Equation (6) shows that the transfer function consists of a fifth-degree polynomial in the denominator and a first-degree polynomial in the numerator. One initial step to confirm that the derived transfer function is correct is to remove the core and the resistive components of the transformer to reduce the circuit to a lossless LCL-filter. This is achieved

by setting the series resistances to zero,  $R_f = R_s = R'_p = 0$  and letting  $R'_c \rightarrow \infty$  and  $L'_m \rightarrow \infty$ , so the transfer function is reduced to the following equation:

$$H_{LCTr} = \frac{I_g}{V_{in}} = \frac{1}{n} \cdot \frac{1}{L_f C_f (L_s + L'_p) s^3 + (L_f + L_s + L'_p) s}. \quad (14)$$

This is essentially the same transfer function as for the LCL-filter in Equation (4), but with the inclusion of the inductors  $L_s$  and  $L'_p$ , and the turns ratio,  $n$ , of the transformer in the denominator.

The resonance frequency of the reduced transfer function in Equation (14) is given by the following equation:

$$\omega_{res,LCTr} = \sqrt{\frac{L_f + L_s + L'_p}{L_f C_f (L_s + L'_p)}}. \quad (15)$$

The Bode plot of the transfer function in Equation (14) is illustrated in Figure 6. The Bode plot is made using the parameter values for the system considered in this paper (see Section 5.2). As can be observed, if the resistances and the core parameters of the system are disregarded, the expected frequency response of the system is in essence the same as the frequency response of the lossless LCL-filter. The resonance frequency calculated using Equation (15) with the parameter values of the considered system is 2300 Hz.

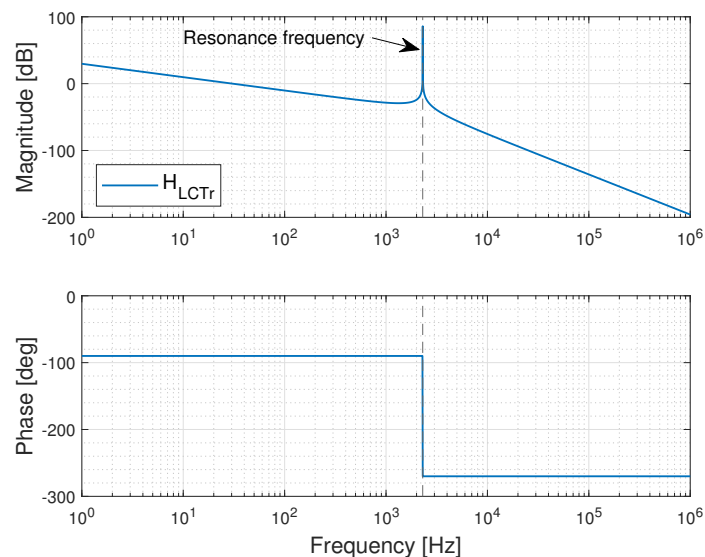


**Figure 6.** Bode plot for the transfer function of a lossless LC-filter and power transformer.

## 5. Method

In this section, the verification process of the transfer function in Equation (6) is presented. The considered electrical system was simulated in LTspice, and the system was experimentally verified with an emphasis on the frequency response. The results will be compared with the analytical solution with the same component values as in the experiments.

### 5.1. Simulations in LTspice

The frequency response was studied using simulations in LTspice with a sine wave generator as the input voltage source and a short-circuited primary side of the transformer to represent the grid. The voltage source was modeled with an internal resistance of 50  $\Omega$  like the function generator used for the experiments. The data from the measurements of resistance and capacitance of the LC-filter have been used, described in Section 5.2.

The output current was compared with the input voltage to produce a Bode plot of the transfer function described in Section 4. Simulations were conducted from 1 Hz to 4 kHz in steps less than 1 Hz in order to capture the expected resonance frequency of 2.3 kHz.

### 5.2. The Filter and Power Transformer Parameters

The LC-filter is a Schaffner FN5040-17-83 rated at 7.5 kW. The construction of the filter is such that it is not possible to access the neutral point of the capacitors. Therefore, to enable the experimental verification of the single-phase circuit, an external capacitor was used in the experiment. The capacitor is an MKP1847H AC Filtering metalized polypropylene film capacitor with a rated capacitance of 10  $\mu$ F. The values used are summarized in Table 1.

The transformer is a three-phase TOFS-7,5 supplied by Tramo ETV. It is rated at 7.5 kVA and 400 V  $\Delta$ /230 V Y with a turn ratio of  $n \approx 1.7$ . For the purpose of the experiment, the transformer was Y-Y connected. The series impedance was determined using a short-circuit test and the core impedance using an open-circuit test. The resistances and reactances determined from the short-circuit and open-circuit tests varied between the phases, and therefore, the mean values of all three phases were used in the model. The measured equivalent series resistance, as seen from the primary side, was divided between the primary and secondary sides using the turns ratio. These measured and calculated values are summarized in Table 1.

**Table 1.** Measured and calculated system parameters for the LC-filter and transformer.

Parameter	Value
<b>LC-filter measured values</b>	
Inductance, $L_f$	2.4 mH
Resistance of inductor, $R_f$	66 m $\Omega$
Capacitance, $C_f$	10 $\mu$ F
<b>Transformer measured values</b>	
Series equivalent resistance	1.4 $\Omega$
Series equivalent inductance	1.8 mH
Core resistance, $R_c$	8225 $\Omega$
Magnetizing inductance, $L_m$	9.22 H
<b>Transformer calculated values</b>	
Primary side series resistance, $R_p$	0.7 $\Omega$
Primary side leakage inductance, $L_p$	0.9 mH
Secondary side series resistance, $R_s$	0.23 $\Omega$
Secondary side leakage inductance, $L_s$	0.3 mH

### 5.3. Experimental Setup of the LC-Filter and Power Transformer for One Phase

Data to investigate the transfer function of the system were collected using the three-phase transformer and the LC-filter. The experimental setup is shown in Figure 7. The transformer was short-circuited on the primary side, and an input voltage was connected to one of the phases of the filter. The input voltage and output current were measured for a frequency range of 1 Hz to 4 kHz in steps according to Table 2. The step size was reduced around the expected resonance frequency.

**Table 2.** Step sizes for the frequency range intervals used in the experimental study.

Frequency Range	Step Size
1 Hz to 10 Hz	1 Hz
10 Hz to 100 Hz	10 Hz
100 Hz to 2100 Hz	100 Hz
2100 Hz to 2400 Hz	20 Hz
2400 Hz to 3000 Hz	50 Hz
3000 Hz to 4000 Hz	500 Hz

Current was measured using a Fluke i310s current clamp set to measure up to 30 A (10 mV/A). Voltage was measured with a differential probe TESTEC TT-SI 9002, set to measure up to 140 V with an attenuation ratio of 1/20. Both the current and voltage measurements were logged using a PicoScope 5443A with a measurement frequency of 1 MHz and a hardware resolution of 14 bits. To reduce the impact of noise on the measurements, an average of 32 waves were used for the voltage and current measurements.

Input voltage was supplied with a function generator GW-instek SFG-1013 with an internal resistance of 50  $\Omega$ . The output of the function generator was also used as a trigger for the PicoScope to obtain a more stable data capture for the averaging function in the PicoScope software.

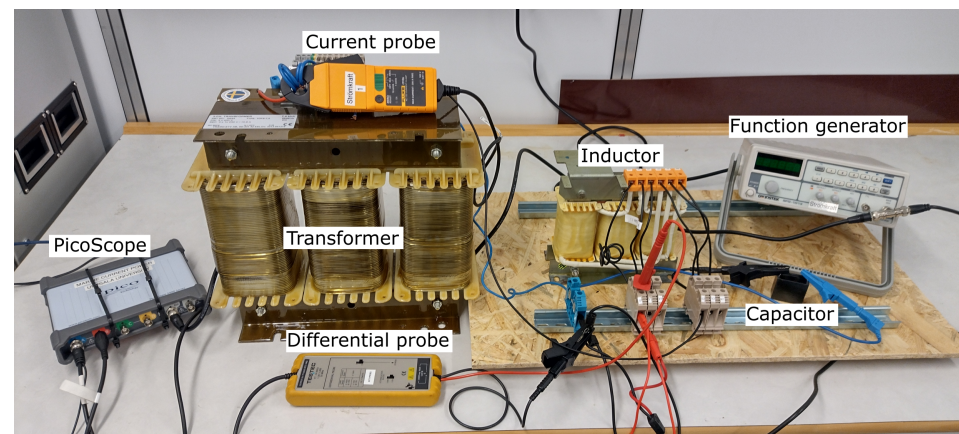


Figure 7. Experimental setup.

## 6. Results

The frequency response of the output current over the input voltage for the analytical solution, simulation, and experiment is shown in the Bode plot in Figure 8. The results from the analytical solution and the simulation overlap almost perfectly. The magnitudes of the experimental values are about 1 dB lower than the simulation and analytical results until the resonance peak and follow the same trend as the analytical and simulation results. After the resonance peak, the difference is less than 0.2 dB at the measurements at 3500 Hz and 4000 Hz. The experimental results exhibit higher attenuation at the resonance frequency, with  $-10.4$  dB for the analytical and simulation and  $-23.8$  dB for the experiment, i.e., a difference of 13.4 dB.

The resonance peak of the analytical solution and the simulation occurs at approximately  $f_0 = 2297$  Hz. The resonance frequency of the measured data is around 2290 Hz to 2300 Hz, i.e., within 0.4% of the simulation and analytical solution. If the shunted part of the transformer equivalent circuit and the resistive parts of the circuit are disregarded, Equation (15) can be used to calculate the resonance frequency of the corresponding lossless LCL-filter. The resonance frequency of a lossless LCL-filter is 2300 Hz, and it can therefore be observed that the frequency of the resonance peak of the system considered in Figure 5 is equivalent to that of a lossless LCL-circuit.

Regarding the phase shift in Figure 8, the measured values follow the analytical and simulation values closely until the resonance frequency is reached. After the resonance frequency is reached, the measured values move towards a value of  $-242^\circ$ , while the analytical and simulation values are around  $-268^\circ$ .

Since the experimental results appear to be more damped than the theoretical results, it is likely that the resistance of the cables and connectors has a dampening effect on the system, which is not incorporated into the model. Other possible sources for the deviation are the following. Regarding the transformer, the average values of the results from the short-circuit and the open-circuit test for all three phases were used, which means the values could have deviated for a specific phase. The parameters of the filter and transformer are also determined at a rated frequency, and in the experiment, a much

larger frequency interval was used. Furthermore, stray capacitances and inductances may influence the frequency response at high frequencies. Finally, a likely source for the deviation is measurement errors arising from the fact that the currents delivered by the function generator are very small, starting from 40 mA for the lowest frequency in the experiment, which makes it difficult to achieve accurate measurements.

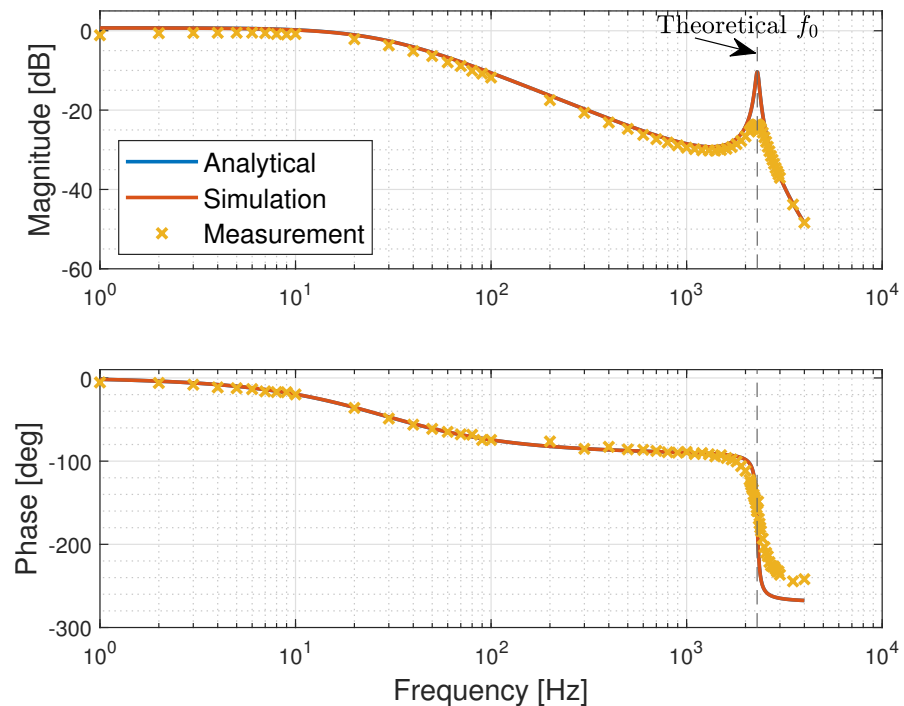


**Figure 8.** Bode plot with the measured data, analytical data, and simulation data. Measurement points are marked with an “x”.

## 7. Conclusions

The transfer function has been derived for an LC-filter connected to a power transformer, which together constitutes an LCL-filter. It is shown that the derived transfer function shows good agreement with LTspice simulations. The analytical and simulation results have been validated with measurements on the corresponding physical circuit for frequencies ranging from 1 Hz to 4 kHz, covering the theoretical resonance frequency. For frequencies below the resonance frequency, the error between the analytical and simulation results and the measurement results is small. Around the resonance frequency, the magnitudes of the measured values are more attenuated than the corresponding simulation and analytical results, which is most likely due to resistances in the system that are not included in the model or measurement errors due to very small currents. For frequencies above the resonance frequency, the error between the analytical and simulation results and the measurements is small with regard to the magnitude. However, the phase shift of the experimentally measured values is smaller than the phase shift of the analytical solution and simulation results above the resonance frequency. From the analytical and simulation results and the measured results, the system can be considered significantly damped. The magnitude of the theoretical resonance peak from the analytical and simulation results is around  $-10.4$  dB and the measured peak is around  $-23.8$  dB. However, the frequency of the resonance peak was from the theoretical results predicted with an error of less than 0.4%.

**Author Contributions:** Conceptualization, C.F. and J.F.; methodology, C.F. and J.F.; software, C.F. and J.F.; validation, C.F. and J.F.; formal analysis, C.F. and J.F.; investigation, C.F. and J.F.; resources, C.F., J.F. and K.T.; data curation, C.F. and J.F.; writing—original draft preparation, C.F. and J.F.; writing—review and editing, C.F.; visualization, C.F. and J.F.; supervision, K.T.; project administration, C.F., J.F.

and K.T.; funding acquisition, J.F. and K.T. All authors have read and agreed to the published version of the manuscript.

**Funding:** This work was supported by STandUP for Energy.

**Data Availability Statement:** Data will be made available on request.

**Conflicts of Interest:** The authors declare that they have no known competing financial interest or personal relationships that could have appeared to influence the work reported in this paper.

## References

1. IEA. *Renewables 2021—Analysis and Forecast to 2026*; Technical Report; International Energy Agency (IEA): Paris, France, 2021.
2. Blaabjerg, F.; Ma, K. Wind Energy Systems. *Proc. IEEE* **2017**, *105*, 2116–2131. [[CrossRef](#)]
3. Teodorescu, R.; Rodriguez, P.; Liserre, M. *Grid Converters for Photovoltaic and Wind Power Systems*, 3rd ed.; John Wiley & Sons, Ltd.: Chichester, UK, 2011.
4. Lundin, S.; Forslund, J.; Carpmann, N.; Grabbe, M. The Söderfors Project: Experimental Hydrokinetic Power Station Deployment and First Results. In Proceedings of the 10th European Wave and Tidal Energy Conference (EWTEC), Aalborg, Denmark, 2–5 September 2013.
5. Apelfröjd, S.; Ekström, R.; Thomas, K.; Leijon, M. A back-to-back 2L-3L grid integration of a marine current energy converter. *Energies* **2015**, *8*, 808–820. [[CrossRef](#)]
6. Forslund, J.; Thomas, K. First Experimental Results of a Grid Connected Vertical Axis Marine Current Turbine using a Multilevel Power Converter. In Proceedings of the 4th Asian Wave and Tidal Energy Conference (AWTEC), Taipei, Taiwan, 9–13 September 2018.
7. Beres, R.; Wang, X.; Blaabjerg, F.; Bak, C.L.; Liserre, M. *A Review of Passive Filters for Grid-Connected Voltage Source Converters*; Institute of Electrical and Electronics Engineers Inc.: Piscataway, NJ, USA, 2014; pp. 2208–2215. [[CrossRef](#)]
8. Han, Y.; Yang, M.; Li, H.; Yang, P.; Xu, L.; Coelho, E.A.A.; Guerrero, J.M. Modeling and stability analysis of LCL-type grid-connected inverters: A comprehensive overview. *IEEE Access* **2019**, *7*, 114975–115001. [[CrossRef](#)]
9. Büyük, M.; Tan, A.; Tümay, M.; Bayindir, K.Ç. Topologies, generalized designs, passive and active damping methods of switching ripple filters for voltage source inverter: A comprehensive review. *Renew. Sustain. Energy Rev.* **2016**, *62*, 46–69. [[CrossRef](#)]
10. Liserre, M.; Blaabjerg, F.; Dell’Aquila, A. Step-by-step design procedure for a grid-connected three-phase PWM voltage source converter. *Int. J. Electron.* **2004**, *91*, 445–460. [[CrossRef](#)]
11. Liserre, M.; Blaabjerg, F.; Hansen, S. Design and control of an LCL-filter-based three-phase active rectifier. *IEEE Trans. Ind. Appl.* **2005**, *41*, 1281–1291. [[CrossRef](#)]
12. Jalili, K.; Bernet, S. Design of LCL Filters of Active-Front-End Two-Level Voltage-Source Converters. *IEEE Trans. Ind. Electron.* **2009**, *56*, 1674–1689. [[CrossRef](#)]
13. Rockhill, A.A.; Liserre, M.; Teodorescu, R.; Rodriguez, P. Grid-Filter Design for a Multimegawatt Medium-Voltage Voltage-Source Inverter. *IEEE Trans. Ind. Electron.* **2011**, *58*, 1205–1217. [[CrossRef](#)]
14. Tripathi, R.N.; Singh, A.; Hanamoto, T. Design and control of LCL filter interfaced grid connected solar photovoltaic (SPV) system using power balance theory. *Int. J. Electr. Power Energy Syst.* **2015**, *69*, 264–272. [[CrossRef](#)]
15. Reznik, A.; Simões, M.G.; Al-Durra, A.; Mueen, S.M. LCL Filter Design and Performance Analysis for Grid-Interconnected Systems. *IEEE Trans. Ind. Appl.* **2014**, *50*, 1225–1232. [[CrossRef](#)]
16. Jayalath, S.; Hanif, M. An LCL-Filter Design with Optimum Total Inductance and Capacitance. *IEEE Trans. Power Electron.* **2018**, *33*, 6687–6698. [[CrossRef](#)]
17. Gurrola-Corral, C.; Segundo, J.; Esparza, M.; Cruz, R. Optimal LCL-filter design method for grid-connected renewable energy sources. *Int. J. Electr. Power Energy Syst.* **2020**, *120*, 105998. [[CrossRef](#)]
18. Dannehl, J.; Wessels, C.; Fuchs, F.W. Limitations of Voltage-Oriented PI Current Control of Grid-Connected PWM Rectifiers with LCL Filters. *IEEE Trans. Ind. Electron.* **2009**, *56*, 380–388. [[CrossRef](#)]
19. Zhang, C.; Dragicevic, T.; Vasquez, J.C.; Guerrero, J.M. *Resonance Damping Techniques for Grid-Connected Voltage Source Converters with LCL Filters—A Review*; IEEE Computer Society: Washington, DC, USA, 2014; pp. 169–176. [[CrossRef](#)]
20. Gomes, C.C.; Cupertino, A.F.; Pereira, H.A. Damping techniques for grid-connected voltage source converters based on LCL filter: An overview. *Renew. Sustain. Energy Rev.* **2018**, *81*, 116–135. [[CrossRef](#)]
21. Hanif, M.; Khadkikar, V.; Xiao, W.; Kirtley, J.L. Two degrees of freedom active damping technique for LCL filter-based grid connected PV Systems. *IEEE Trans. Ind. Electron.* **2014**, *61*, 2795–2803. [[CrossRef](#)]
22. Eldeeb, H.; Massoud, A.; Abdel-Khalik, A.S.; Ahmed, S. A sensorless Kalman filter-based active damping technique for grid-tied VSI with LCL filter. *Int. J. Electr. Power Energy Syst.* **2017**, *93*, 146–155. [[CrossRef](#)]
23. Valdivia, V.; Pleite, J.; Zumel, P.; González, C.; Lázaro, A. Three Phase LCL Filter and Transformer with Integrated Magnetics for Grid Connected Converters. In Proceedings of the 34th Annual Conference of IEEE Industrial Electronics, Orlando, FL, USA, 10–13 November 2008.
24. Valdivia, V.; Pleite, J.; Zumel, P.; González, C. Improving the design of integrated magnetics for power electronics systems. In Proceedings of the 2008 IEEE Power Electronics Specialists Conference, Rhodes, Greece, 15–19 June 2008.

25. Venkatramanan, D.; John, V. Integrated higher-order pulse-width modulation filter-transformer structure for single-phase static compensator. *IET Power Electron.* **2013**, *6*, 67–77. [[CrossRef](#)]
26. Pleite, J.; Valdivia, V.; Zumel, P.; Gonzalez, C. Transformer and Series Inductance Integration for Harmonic Filtering in PWM Inverters Based in a Simple Design Procedure. In Proceedings of the 2007 IEEE International Symposium on Industrial Electronics, Vigo, Spain, 4–7 June 2007; pp. 1201–1206. [[CrossRef](#)]
27. Khan, D.; Hu, P.; Habib, S.; Waseem, M.; Lin, Z.; Ahmed, E.M. A resonant damping control and analysis for LCL-type grid-connected inverter. *Energy Rep.* **2022**, *8*, 911–928. [[CrossRef](#)]
28. Peña-Alzola, R.; Liserre, M.; Blaabjerg, F.; Sebastián, R.; Dannehl, J.; Fuchs, F.W. Analysis of the passive damping losses in LCL-filter-based grid converters. *IEEE Trans. Power Electron.* **2013**, *28*, 2642–2646. [[CrossRef](#)]
29. Paul, C.R. *Introduction to Electromagnetic Compatibility*, 2nd ed.; Wiley-Interscience: Hoboken, NJ, USA, 2006.

**Disclaimer/Publisher’s Note:** The statements, opinions and data contained in all publications are solely those of the individual author(s) and contributor(s) and not of MDPI and/or the editor(s). MDPI and/or the editor(s) disclaim responsibility for any injury to people or property resulting from any ideas, methods, instructions or products referred to in the content.